Vietnam Journal of Earth Sciences, 47(1), 1-15, https://doi.org/10.15625/2615-9783/21329

Vietnam Journal of Earth Sciences
https://vjs.ac.vn/index.php/jse

A numerical experiment on hail forecast: Hailstorms on 17 March 2020 in western North Vietnam

Doan Manh Duy[1], Nguyen Minh Truong[1*], Nguyen Vinh Thu[2], Hoang Thi Thanh Thuat[2]

[1]*Faculty of Meteorology Hydrology and Oceanography, VNU University of Science*
[2]*Vietnam National Center for Meteorological and Hydrological Network*

Received 01 November 2023; Received in revised form 08 May 2024; Accepted 12 August 2024

ABSTRACT

This study utilized the Weather Research and Forecast (WRF) model to forecast hail induced by the hailstorms on 17 March 2020 in western North Vietnam, using two microphysical schemes: the Thompson and Morrison schemes. Assessment of the WRF skill in predicting hail coverage and intensity was done for two predicted indices, namely UH (Updraft Helicity) and CTG (Column Total Integrated Graupel). Two predicted variables are D_{Th} (hail diameter given by WRF using the Thompson Hail Algorithm) and D_{Hc} (hail diameter given by the HAILCAST submodel in WRF). The predicted hail coverage and intensity were compared with the products given by the Pha Din radar's Hail Size Discrimination Algorithm (HSDA) for three categories: small, large, and giant hail size. Using the Morrison scheme, the WRF model indicates that the hail-coverage forecast skills of UH, CTG, and D_{Hc} are highest, with an insignificant difference at the horizontal scale larger than 60 km. However, the D_{Hc} variable given by the Morrison scheme provides the most successful forecast for both hail size and coverage compared with the HSDA products and field reports. This is because HAILCAST considers kinematic and microphysical processes to predict maximum hail size at the surface. The predicted hailstorms could occur in environments with moderate convective available potential energy but require robust moisture flux convergence over high mountains.

Keywords: Hail, HSDA, thunderstorm indices, HAILCAST.

1. Introduction

Hail induced by hailstorms is one of the most destructive weather phenomena in many world areas (Allen et al., 2020). The impacts of hail on infrastructure, the economy, and human life have increased quickly as society continues to develop. In addition to the achievements of traditional forecasting methods, convection-allowing numerical weather prediction (NWP) models based on high computing capacity have become valuable tools for warning and forecasting severe weather events. Current convection-allowing models (CAMs) are capable of resolving convective structures at scales below 3 kilometers (Labriola et al., 2019a; Luo et al., 2017), among which the Weather Research and Forecasting (WRF) model (Skamarock et al., 2019) is the most widely used CAM. The model can also be applied to research in other fields, such as hydrology, atmospheric chemistry, and climate research (Powers et al., 2017). However, numerical hail prediction remains one of the most

*Corresponding author, Email: Truongnm@vnu.edu.vn

challenging meteorological problems due to the complicated thermodynamic processes in small spatial and temporal scales (Melcón et al., 2017).

With the development of NWP models in the latest decades, significant progress has been made in forecasting extreme weather events induced by severe convection. For example, *Updraft Helicity* (UH) index (Stull 2017) has been used in operational forecasting of severe weather in the United States, including hail and hailstorms (Sobash et al., 2020). UH appears to be the most reliable predictor of large hail coverage (hailstone diameter from 25 to 50 mm) and exhibits the highest skill in hail prediction compared with other predicted indices in various scales and model options (Gagne et al., 2017). Another surrogate index for hail prediction is *Column-Integrated Total Graupel* (CTG), which strongly correlates with ground-based hail size measurements (Gagne et al., 2017). However, CTG has lower hail prediction skills than UH due to its sensitivity to microphysical schemes (MP) but insensitivity to dynamic environmental changes (Labriola et al., 2019a).

In addition to surrogate hail forecasting, several methods have been developed to estimate surface hail size using NWP products. The *Thompson hail algorithm* (Snook et al., 2016) computes the maximum diameter of hydrometeor droplets given by MP schemes, thereby estimating largest hailstones that can reach the surface. The algorithm has shown high skill in predicting hail coverage for specific MP schemes (Snook et al., 2016; Labriola et al., 2019a; Labriola et al., 2020). Another method employed for hail size forecasting is the *HAILCAST model*, initially developed for sounding observations as a one-dimensional but physically based model (Adams-Selin and Ziegler, 2016). HAILCAST has also been modified to be embedded within CAMs as a submodel to simulate hailstone growth rate based on physical relationships, as long as convection meets certain conditions (Brimelow et al., 2002; Jewell et al., 2009). The HAILCAST submodel has been developed and applied to operation at the American Storm Prediction Center (Brimelow et al., 2002; Jewell et al., 2009), satisfying various real case experiments. In recent years, it has also been integrated into the WRF model and shown its ability to predict hail with high skill (Adams-Selin et al., 2019).

Hail observation remains challenging, even with modern radar or satellite methods. Several methods have been developed to estimate hail size based on radar data, including the *Hail Size Discrimination Algorithm* (HSDA, Ryzhkov et al., 2013). HSDA classifies hailstone diameters into three categories: small, large, and giant hail. Although this method is only applicable to dual-polarization radar, it has been used as a hail observation index to evaluate the hail prediction skill of NWP models (Labriola et al., 2019a; Snook et al., 2016; Ortega et al., 2016; Labriola et al., 2017). Recently, the weather radar network in Vietnam has been expanded and upgraded to dual-polarization radars, initially satisfying demands in research and operational forecasting. The latest applications of radar data include rainfall estimation (Thanh et al., 2018; Hoat et al., 2023; Thang et al., 2013), thunderstorm forecasting (Quyet et al., 2011), and data assimilation for NWP models (Minh et al., 2023).

Hailstorms can occur in most regions of Vietnam, particularly in mountainous areas during transition seasons. However, there have been limited studies on this phenomenon, mainly due to the lack of hail observation data. Regarding numerical studies on hailstorms, Thang et al. (2020) analyzed the hailstorms occurring on 24–25/01/2020 in northern Vietnam. Duy and Truong (2022) conducted

numerical experiments using two surrogate storm indices (UH and CTG) to predict the same hailstorms. Their results demonstrate that NWP models could be effectively utilized for hail prediction in Vietnam. In addition to the recent stable quality of the Vietnamese radar network, the studies above stimulate us to investigate hail prediction in Vietnam. Therefore, this study aims to conduct numerical experiments using two MP schemes, namely the Thompson (MP08, Thompson et al., 2008) and Morrison (MP10, Morrison et al., 2005) schemes, on the hailstorms occurring on 17 March 2020 in western North Vietnam. These two MP schemes have often been used in hailstorm research (e.g., Labriola et al., 2019a; 2020). Analyses of the WRF skill in predicting hail are performed for two predicted indices, namely UH and CTG, and two variables, that is, D_{Th} (i.e., hail diameter given by WRF using the Thompson hail algorithm) and D_{Hc} (i.e., hail diameter given by the HAILCAST submodel in WRF), by comparing them with the HSDA hail categories. The following section introduces the methodology and data used in this study. Results are given in section 3, and the last section presents the discussion and concluding remarks.

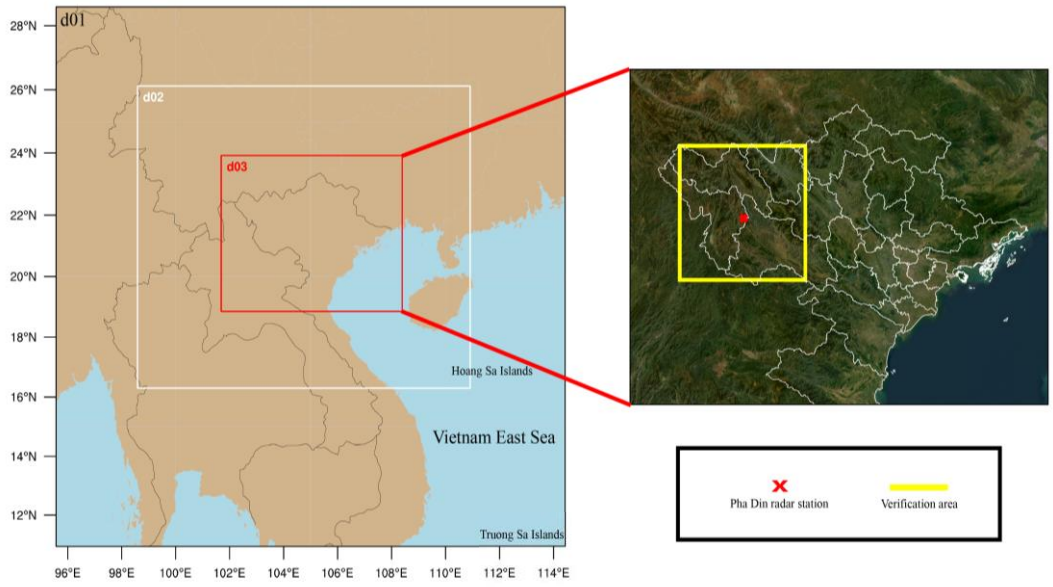

Figure 1. Nested domain configuration (left) and the finest domain (right). Yellow rectangular is the area used to verify predictions. Red X indicates the Pha Din radar station.

2. Methodology and data

2.1. Hailstorms on 17 March 2020 in western North Vietnam

From the evening of 17 March to the early morning of 18 March 2020, widespread hailstorms occurred in western North Vietnam. Hail was reported in various locations, including Si Ma Cai district (Lao Cai) around 19:00; Sin Ho, Tam Duong, and Lai Chau city at 20:50 local time on 17 March 2020, with reported hail size of 3–4 cm in diameter. Other areas, such as Son La, Yen Bai, Phu Tho, Tuyen Quang, and Bac Kan, also experienced these hailstorms. These severe hailstorms damaged 3188 houses, 1028 hectares of crops, and 271 hectares of fruit trees. The total damage is approximately 14.06 billion Vietnamese Dong (VMHA, 2020). Field reports on hail diameter and timing are summarized in Table 1.

Table 1. Summary of field reports on hail locations, timing (local time), and size

Hail report	Location	Reported time	Hail size
Muong Te, Lai Chau	22.47°N-102.84°E	18:00	1.0–1.5 cm
Sin Ho, Lai Chau	22.47°N-103.13°E	20:50	2.0–3.0 cm
Tam Duong, Lai Chau	22.33°N-103.54°E	20:50	3.0–4.0 cm
Lai Chau city, Lai Chau	22.39°N-103.47°E	20:50	2.0–3.0 cm
Bac Ha, Lao Cai	22.54°N-104.29°E	19:00	None
Si Ma Cai, Lao Cai	22.68°N-104.27°E	19:00	2.0–3.0 cm
Tan Quang, Ha Giang	22.49°N-104.86°E	23:00	None
Luc Yen, Yen Bai	22.11°N-104.76°E	23:00	1.0–1.5 cm
Moc Chau, Son La	20.94°N-104.60°E	17:30	2.0–3.0 cm
Moc Chau, Son La	20.91°N-104.54°E	17:30	2.0–3.0 cm
Doan Hung, Phu Tho	21.62°N-105.18°E	None	None
Cam Khe, Phu Tho	21.41°N-105.13°E	None	None

2.2. Radar data and HSDA

This study uses data from the recently installed Pha Din (Dien Bien) radar, a Doppler C-band dual-polarization radar (WRM200). The Pha Din radar station is 1470 meters above sea level and surrounded by mountains that could introduce noise in raw data, especially at low elevation angles. Filtering software provided by the radar manufacturer was employed to address this noise.

Radar data at 10-minute resolution was processed using the Pyart library in Python, as described by Helmus et al. (2016). The HSDA index was computed based on the Hydrometeor Classification Algorithm (HCA, Park et al., 2009) and three indices derived from dual-polarization radar data to diagnose dominant hydrometeor species, including differential reflectivity, correlation coefficient, and differential phase (Ryzhkov et al., 2013). HSDA classifies hail diameters into three categories: small hail (SH, diameter from 5 to 25 mm), large hail (LH, diameter between 25 and 50 mm), and giant hail (GH, diameter exceeding 50 mm) according to the study of Labriola et al. (2019a). Radar data at the lowest elevation angle of 0.5 degrees were chosen for HSDA due to its superior accuracy in hail measurements (Ortega et al., 2016). In this study, the HSDA hail categories were computed for a grid mesh at 1.5 km resolution to facilitate comparisons with the WRF model products (as described later in subsection 2.3).

2.3. Model configuration and predicted indices and variables

This study employed the WRF model version 4.3.3 (Skamarock et al., 2019) with three nested grids of 13.5, 4.5, and 1.5 km grid spacing and 51 vertical levels. The third grid is quite fine to resolve the hailstorms (Luo et al., 2017; Labriola et al., 2019a). Initial and boundary conditions were Global Forecast System data at 0.25-degree and 03-hour resolution. The model was initialized at 12:00 UTC on 16 March 2020, approximately 24 hours before the event, and run for 48 hours. Table 2 summarizes the parameterization schemes used in this study.

The UH index is computed following Kain et al. (2008):

$$\mathrm{UH} = \int_{z1}^{z2} w\zeta dz \qquad (1)$$

where UH represents the updraft helicity (m^2s^{-2}), w is the vertical velocity (ms^{-1}), ζ is the relative vorticity (s^{-1}), z1 = 2 km, and z2 = 5 km. CTG is obtained as the integrated product of the graupel mixing ratio q_{graup} and the air density ρ_{air} throughout the air column:

$$\mathrm{CTG} = \int_{z0}^{z3} q_{graup}\rho_{air} dz \qquad (2)$$

where z0 and z3 indicate the surface and model top, respectively.

Table 2. Parameterization schemes used in this study

Parameterization	Scheme	Note
Microphysics	Thompson	MP08
	Morrison	MP10
Longwave radiation	RRTM	
Shortwave radiation	Dudhia	
Planet boundary	YSU	
Land-surface option	Thermal diffusion scheme	
Cumulus	Kain-Fritsch	Only used in 1st nest

The HAILCAST submodel estimates hail size at each time step, continuing until hailstones reach the ground. The resulting hail prediction is passed back to WRF, which stores that data (i.e., D_{Hc}) and then moves to its next time step (Adams-Selin and Ziegler, 2016). For the D_{Th} variable, hydrometeor diameters are solved by MP schemes using a Particle Size Distribution function (Ulbrich et al., 1983), which is then used by the Thompson hail algorithm to estimate the maximum hail size at each grid point provided that the total number of hail concentration reaches a minimum threshold of at least 10^{-4} m^{-3} or one hailstones is found within a 100×100 m patch with a depth of 1 m (Labriola et al., 2019a). Taking the size at the surface layer yields the maximum hail size (D_{Th}). Unlike the two thunderstorm indices, which are not hail-size variables, D_{Th} and D_{Hc} are available hail-size variables of the WRF model. The predicted variables D_{Th} and D_{Hc} and indices UH and CTG are subsequently converted into three hail-intensity categories as given in Table 3 based on Labriola et al. (2019a), who used the thresholds of Gagne et al. (2017), which are then compared with the HSDA categories.

To examine environmental conditions given by the WRF model, which are favorable for the predicted hailstorm formation and development, convective available potential energy (CAPE) is used along with vertically integrated moisture flux convergence (VIMFC, Banacos and Schultz, 2005; Zomeren and Delden, 2007) in the surface-300 hPa layer written as:

$$\mathrm{VIMFC} = -\frac{1}{g}\int_{300hPa}^{P_{sfc}}\left(\frac{\partial uq}{\partial x}+\frac{\partial vq}{\partial y}\right)dp \quad (3)$$

P_{sfc} is the surface pressure, and u and v are the zonal and meridional wind.

Table 3. Three hail categories for the predicted indices and variables

Indices/variables	Small hail SH (> 5 mm)	Large hail LH (25–50 mm)	Giant hail GH (> 50 mm)
Updraft helicity (UH)	UH > 50 $m^2.s^{-2}$	UH > 75 $m^2.s^{-2}$	UH > 150 $m^2.s^{-2}$
Column Total integrated Graupel (CTG)	CTG > 15 $kg.m^{-2}$	CTG > 25 $kg.m^{-2}$	CTG > 50 $kg.m^{-2}$
Thompson hail algorithm (D_{Th})	D > 5 mm	D > 25 mm	D > 50 mm
HAILCAST submodel (D_{Hc})	D > 5 mm	D > 25 mm	D > 50 mm

2.4. Verification method

To evaluate skill in predicting the spatial coverage of field variables, the Fraction Skill Score (FSS) can be utilized (Roberts and Lean, 2008). FSS is computed as the ratio of the mean square error (MSE) and reference mean square error (MSEref).

$$\mathrm{MSE}_{(n)} = \frac{1}{N_x N_y}\sum_{i=1}^{N_x}\sum_{j=1}^{N_y}\left[O_{(n)i,j} - M_{(n)i,j}\right]^2 \quad (4)$$

$$\mathrm{MSE}_{(n)\mathrm{ref}} = \frac{1}{N_x N_y}\left[\sum_{i=1}^{N_x}\sum_{j=1}^{N_y} O_{(n)i,j}^2 + \sum_{i=1}^{N_x}\sum_{j=1}^{N_y} M_{(n)i,j}^2\right] \quad (5)$$

$$\mathrm{FSS}_{(n)} = 1 - \frac{\mathrm{MSE}_{(n)}}{\mathrm{MSE}_{(n)\mathrm{ref}}} \quad (6)$$

where $O_{(n)i,j}$ and $M_{(n)i,j}$ are respectively the observed and predicted fractions for a square of length n, which are computed following the formulations in Roberts and Lean (2008). N_x and N_y are the domain sizes. A random forecast probability, f_0, is the ratio of the observation area to the domain area. FSS is considered skillful if it exceeds threshold L defined by:

$$L = 0.5 + \frac{f_0}{2} \quad (7)$$

When the neighborhood radius n is zero,

FSS corresponds to point evaluation. Conversely, as *n* increases, correct prediction increases while MSE decreases, increasing the FSS skill score. The index describes spatial similarity and distance errors of forecasts compared with observations, making it particularly suitable for verifying the predicted coverage of individual mesoscale events, such as convective rainfall (Mittermaier, 2021) and hail (Luo et al., 2018; Labriola et al., 2019a, Labriola et al., 2019b; Wu et al., 2022).

3. Results and discussion

3.1. HSDA hail coverage and categories

Organized in the form of mesoscale convective systems (MCSs), radar reflectivity exceeding 55 dBZ demonstrates the existence of the thunderstorms over Sin Ho, Tam Duong, and Lai Chau City around 20:50 local time on 17 March 2020 (Fig. 2a), where hail sizes were reported to be 3–4 cm in diameter as mentioned above. Another area of high reflectivity (approximately 55 dBZ) can be seen over Son La province. At the same time, the HCA rain categories suggest the occurrence of hailstorms surrounded by heavy rain in Lai Chau-Lao Cai, Son La, and Ha Giang provinces (Fig. 2b). However, the area of hail in Ha Giang is erroneous as discussed below, because reflectivity is too low to produce hailstorms.

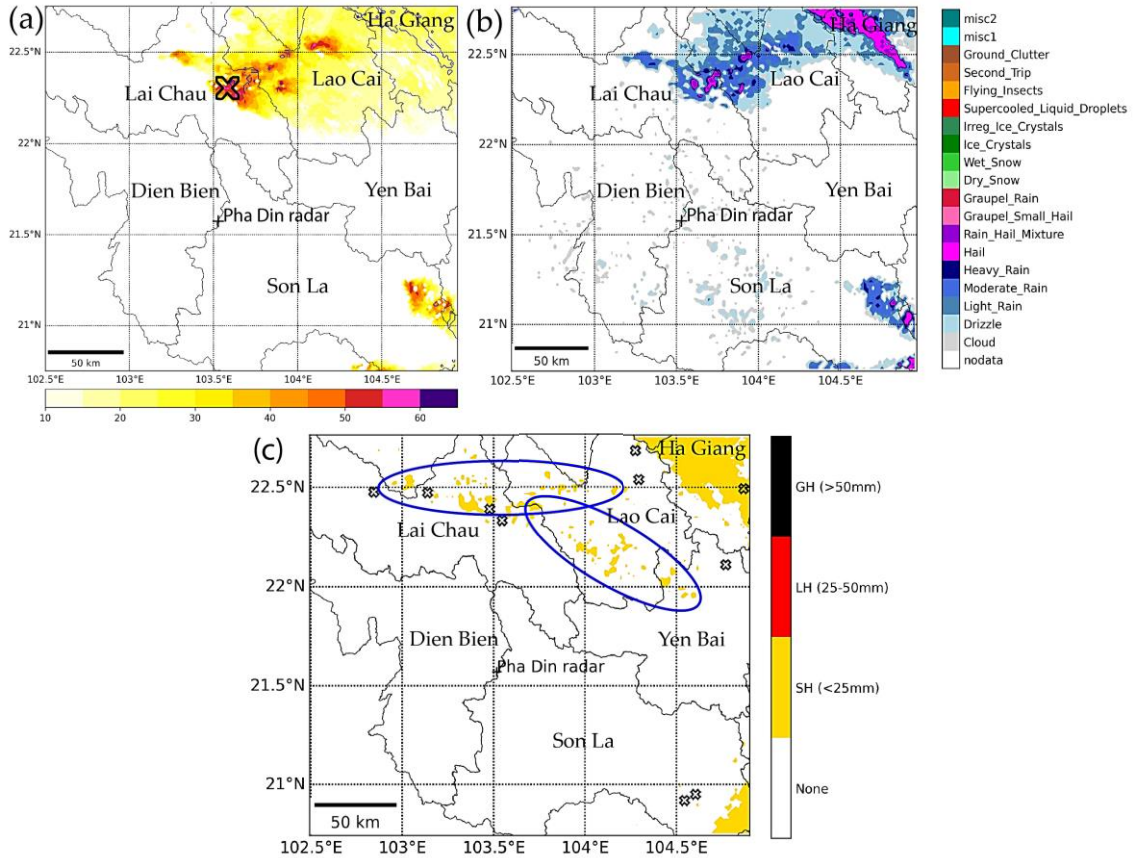

Figure 2. Reflectivity (a) and the HCA rain categories (b) at 20:50 local time on 17 March 2020 given by the Pha Din radar. 5-hour maximum HSDA hail intensity in 19:00–24:00 local time on 17 March 2020 (c). The HSDA hail categories include small hail (SH), large hail (LH), and giant hail (GH). Open X denotes reported hail locations. + indicates the Pha Din radar station

The HSDA hail coverage indicates that the hailstorms induce two main hail swaths in the west-east direction in Lai Chau-Lao Cai provinces and the northwest-southeast direction in Lao Cai-Yen Bai provinces in 19:00–24:00 local time on 17 March 2020 (Fig. 2c). These two swaths are organized as local hail centers with 5–10 km width. It is worth noting that HSDA gives a broad and solid hail area in Ha Giang province. Similarly, HSDA detected a dense area of hail over Son La. It is almost impossible for hail to occur in that way. It seems likely that HSDA does not work well for large distances from the Pha Din radar station to the two provinces. Ortega et al. (2009) suggested that HSDA can reliably estimate hail size up to a radius of about 120 km from the radar station. Moreover, although HSDA well depicts hail coverage that is in good agreement with the reported hail locations, it is essential to note that it categorizes hail intensity as small hail only, whereas reported hail sizes are basically in the range of 20–30 mm (Table 1). It is likely that the HSDA algorithm is not as exact as expected, especially over complex mountains where radar beams should be blocked or jammed, requiring the rejection of deception radar data. Therefore, the HSDA hail coverage west of 104.5°E is used to evaluate hail coverage prediction only (i.e., we avoid uncertainties in the HSDA hail coverage over Son La and Ha Giang).

3.2. Hail timing, coverage, and intensity forecasts

To estimate timing errors of the predicted hailstorms compared with the observations, maximum reflectivity, and hail diameter in 1-hour intervals, in which the hailstorms are detected by the observations and HAILCAST submodel using the MP08 and MP10 schemes, are exhibited in Fig. 3. Accordingly, the radar observes the hailstorms at 20:00–21:00 in Lai Chau-Lao Cai and Son La (Fig. 3e), while HAILCAST recognizes them in Son La (Lai Chau-Lao Cai) at 19:00–20:00 (22:00–23:00) local time on 17 March 2020 as shown in Fig. 3a, b (Fig. 3c, d). Similar timing errors are found with the other predicted indices and variables (not shown). This is perhaps not surprising because NWP models can probably predict thermodynamic environments favorable for the development of severe thunderstorms but cannot precisely predict individual hailstorms evolving in space and time, especially over complex terrains, due to inherent uncertainties. Predicted hail fields, such as coverage and intensity in 1-hour intervals, are almost meaningless; therefore, their maxima over several hours are usually used instead (Adams-Selin et al., 2019). For this reason, hail field maxima in 19:00–24:00 local time on 17 March 2020, when the hail events were observed, are used to analyze hail predictability to the west of 104.5°E, as mentioned above.

Figure 4 exhibits all four indices and variables induced by the two microphysical schemes (i.e., eight forecasts), which indicate hail occurrence, but their coverage and intensity differ significantly. Generally, each microphysical scheme produces similar hail swaths among the four forecasts, but coverage and intensity are still more or less different.

Overall, it can be inferred that MP08 predicts more hailstorms than MP10. The UH index could be high even in non-severe thunderstorms, resulting in the largest number of predicted hail swaths compared with the other index and variables (Figs. 4a, e). Notably, the observed hail swaths in Lai Chau-Lao Cai province are reasonably captured by all eight forecasts compared to the HSDA product (Fig. 2c), except for some centers west of 103.5°E. In addition, it is necessary to emphasize hail areas in Ha Giang and Son La province, as given by the D_{Hc} variable (Figs. 4d, h), whose counterparts are reported in the field. It is a pity that MP10-D_{Hc} cannot predict the hail swath in Lao Cai-Yen Bai (Fig. 4h) as MP08-D_{Hc} and MP08-D_{Th} do (Figs. 4c, d). It is necessary to emphasize that no NWP

model can predict MCSs precisely as shown by observations. Each microphysical scheme gives similar hail swaths in space because deep convection in hailstorms is expected to have high updraft velocity, high UH, and high content of hydrometeors in the solid phase. An exception is the MP10-D_{Th} case (Fig. 4g), in which hail coverage is extremely small, whereas MP08-D_{Th} produces remarkably wider but shorter hail swaths and areas compared with the other indices and variables. This again implies the essential role of microphysical schemes in predicting hail (Luo et al., 2018).

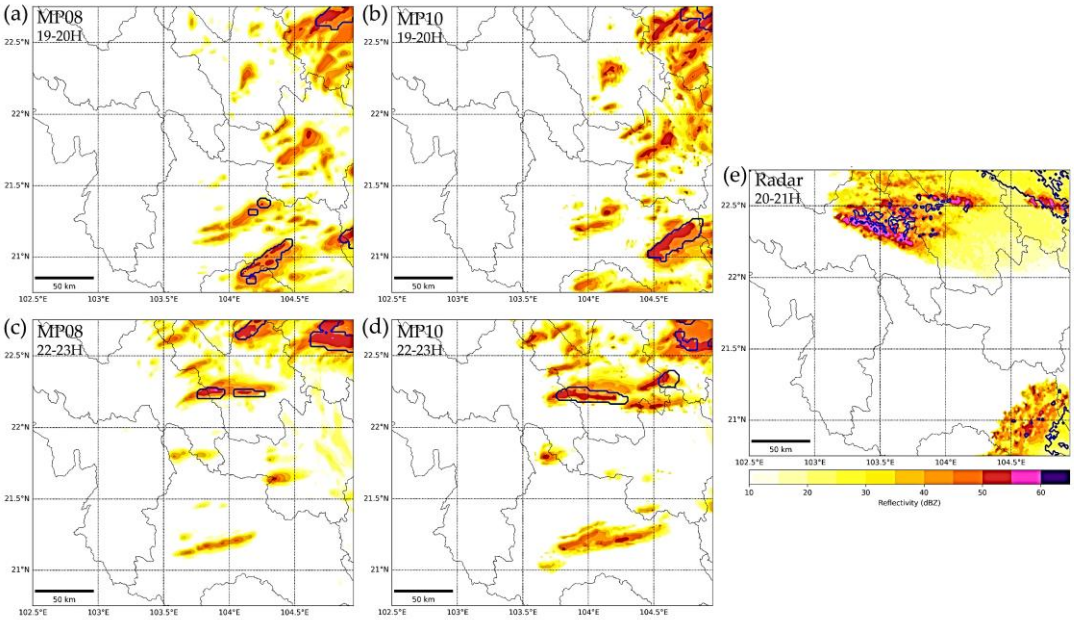

Figure 3. Maximum reflectivity (color shades, dbZ) and 5-mm hail diameter (blue curves) in 1-hour intervals detected by the HAILCAST submodel (a)–(d) and radar HSDA (e)

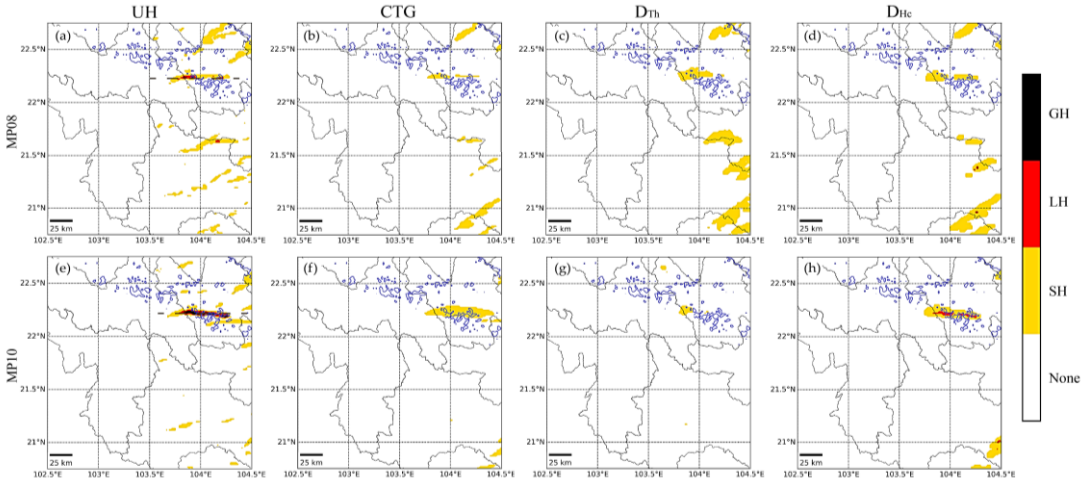

Figure 4. Forecasts of hail coverage and intensity in three categories, SH, LH, and GH given by (a)–(e) UH, (b)–(f) CTG, (c)–(g) D_{Th}, and (d)–(h) D_{Hc} in 19:00–24:00 local time on 17 March 2020, using MP08 and MP10. Blue contours are 5-mm HSDA hail diameter in the 5-hour interval from 19:00–24:00 local time on 17 March 2020. Brown dashed lines in (a) and (e) indicate positions of vertical-longitude sections in Fig. 7

In terms of hail intensity, the MP08-UH forecast shows the LH category (Fig. 4a) while the MP10-UH one can be the GH category (i.e., intensity overestimated in comparison to the field reports, Fig. 4e). Forecasts by CTG and D_{Th} indicate the occurrence of the SH category only (Figs. 4b, c, f, g). In contrast, the HAILCAST submodel suggests several LH centers and swaths. For example, the MP08 scheme predicts two local LH centers in Son La province and adjacent areas (Fig. 4d), which do not coincide with the most robust UH centers in Figure 4a. It is noteworthy that when MP10 is used, the HAILCAST submodel also predicts large hail along the main swath in Lai Chau-Lao Cai as in the MP08-UH case, and a large hail center in Son La as given in the MP08-D_{Hc} case (Fig. 4h), both of which appear to be in best agreement with the radar observations and field reports on hail coverage and intensity.

3.3. Verification of the predicted hail coverage

In this study, we verify forecast skill in predicting hail coverage (i.e., the occurrence of hail in space) of the predicted indices and variables, using the FSS index, which indicates spatial similarity between the observations (i.e., HSDA) and forecasts in 19:00–24:00 local time on 17 March 2020. The skill threshold of the FSS index is L = 0.5504 according to Eq. (7) in this case (Fig. 5), which is somewhat smaller than that in Labriola et al. (2019a) because fractional hail coverage is abnormally large in Labriola et al. (2019a).

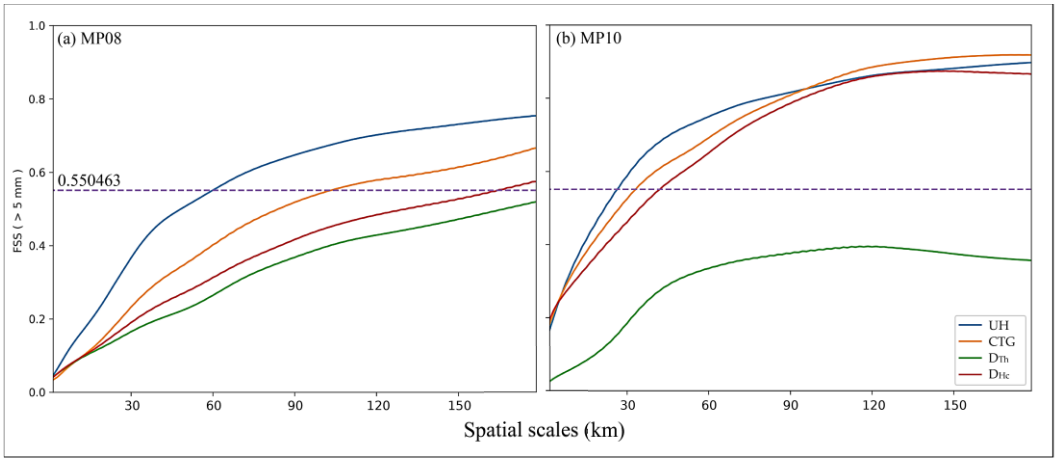

Figure 5. FSS of the predicted indices and variables for hail occurrence threshold (hail diameter > 5 mm) of MP08 (a) and MP10 (b) in 19h00–24:00 local time on 17 March 2020. Dashed lines are skill threshold

Figure 5 shows that MP10 gives remarkably higher skill, except that of the D_{Th} variable, but much smaller skill-attaining scales (Fig. 5b) compared to MP08 (Fig. 5a), suggesting its capability of hail prediction. Specifically, in the MP08 case, the UH index has skill on scales > 60 km, and the corresponding number of the CTG index is about 100 km in the horizontal space. The D_{Hc} variable has no skill until scales get larger than the skill-attaining scale of approximately 165 km (Fig. 5a). For the MP10 scheme, the two indices UH and CTG and variable D_{Hc} attain skill on a scale > 25–45 km. The reason is that although both schemes are double-moment schemes, MP08 does not predict the total number concentration of clouds, snow, and graupel. Like the MP08 case, the UH index given by MP10 has a skill that quickly increases with increasing scale to get the

smallest skill-attaining scale of about 25 km. The CTG index and D_{Hc} variable achieve slightly larger skill-attaining scales but have skill equivalent to the UH index on scales > 90 km. Perhaps surprisingly, the D_{Th} variable has no skill in the MP08 and MP10 cases. The total failure of D_{Th}, a standard variable of the WRF model, is clarified in the following subsection.

3.4. Mechanisms

3.4.1. Environmental conditions

We first explore environmental conditions favorable for the predicted hailstorm formation and development. The HAILCAST submodel using the MP10 scheme shows that the predicted hailstorms do not require strong CAPE, as illustrated in Fig. 6. Accordingly, CAPE is kept moderate with a magnitude slightly larger than 1250 j.kg^{-1} before and when the hailstorms occur in Lai Chau-Lao Cai (Fig. 6a, b), which is reduced afterward (Fig. 6c). CAPE in this study is, thus, of the same order as that in Luo et al. (2018) but much smaller than that in Luo et al. (2017). This implies that CAPE may vary significantly from case to case, depending on specific situations. It is worth mentioning that the hailstorms do not originate in areas with CAPE larger than 1725 j.kg^{-1} but in regions with remarkably strong VIMFC and terrains higher than 1500 m above mean sea level. Therefore, it should be noted here that CAPE is just a necessary condition while VIMFC and lifting mechanism by high terrains are crucial sufficient conditions. Figure 6 further suggests that very strong VIMFC centers along the leading edge of the hailstorms help the whole system propagate eastward.

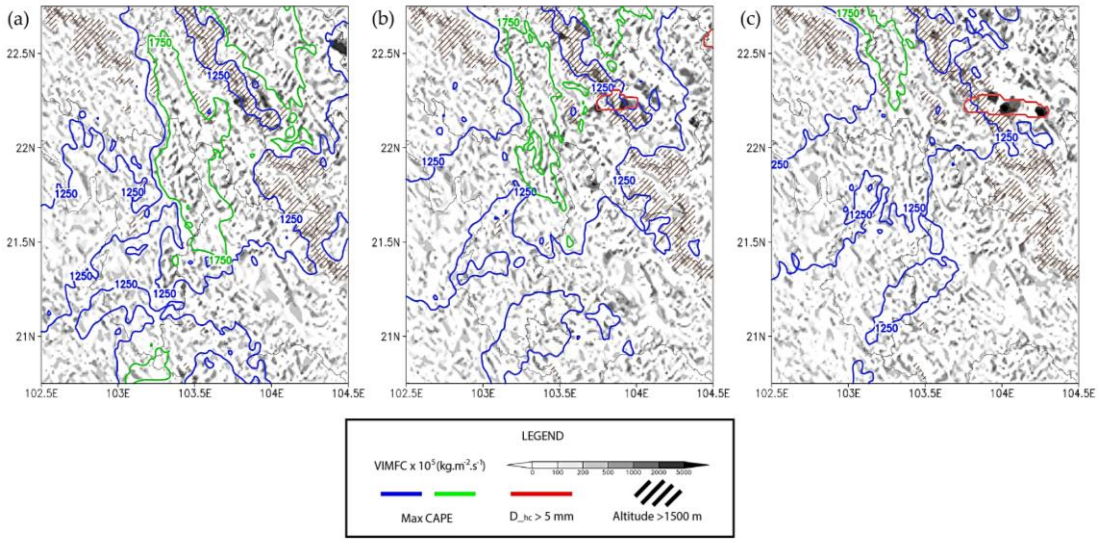

Figure 6. Surface–300 hPa VIMFC (color shades, ×10^5 kg.m^{-2}.s^{-1}), CAPE (blue and green curves, j.kg^{-1}), and 5-mm D_{Hc} (red curves) at 21:00 (a), 22:00 (b), and 23:00 (c) local time on 17 March 2020. Brown slashes indicate terrains higher than 1500 m above mean sea level

3.4.2. Updraft velocities and hydrometeors

In this subsection, vertical-longitude sections are shown to analyze further hailstorm characteristics induced by MP08 and MP10 at 23:00 local time on 17 March 2020 when the two schemes predict the strongest hailstorms. Figure 7 indicates that

MP10 could result in much stronger updraft velocities in the main convective cells with much larger horizontal and vertical scales, up to 200 hPa, compared with MP08. This is consistent with Li et al. (2015) and Van et al. (2013). Conversely, MP08 generates stronger secondary convective cells, for example, on the eastern side of the section. It is not surprising, therefore, that the UH index given by MP10 leads to more intensive hail because UH is physically proportional to updraft velocity. In contrast, the UH index given by MP08 potentially produces more but weaker hail centers, as seen in Fig. 4.

For the distribution of hydrometeors in the main predicted hailstorms, MP08 tends to simulate dense graupel areas evolving below 500 hPa, which extend downward to the surface over high terrains and overlap with wider areas of rain beneath (Fig. 7a). This distribution of hydrometeors keeps graupel particles from melting and evaporating as they fall in a saturated environment. In contrast, MP10 simulates denser graupel areas in much wider horizontal scales, which exist above the 500-hPa level and nearly do not coincide with narrower areas of rain below (Fig. 7b), leading to the melting and evaporation of graupel particles while falling in unsaturated environments (Li et al., 2015). These can result in opposite situations, that is, MP10 generates larger CTG and thereby causes stronger and wider main hail swath in comparison to MP08 (Figs. 4b, f). Conversely, the variable D_{Th} computed from the MP10 scheme shows very small hail coverage compared with MP08 (Figs. 4c, g).

The HAILCAST submodel first checks conditions on updraft velocity to decide if a hailstorm is probable, and it can, therefore, eliminate weaker convective cells in the two UH cases (Figs. 4a, e). On the other hand, HAILCAST computes hail size using contents of hydrometeors, especially graupel, in the air column and, therefore, avoids the disadvantages of the D_{Th} variable that uses graupel content at the lowest model level to predict hail diameter. That is why MP10, which produces stronger main convective cells than MP08, can help HAILCAST to give the best forecast, as shown in subsection 3.2.

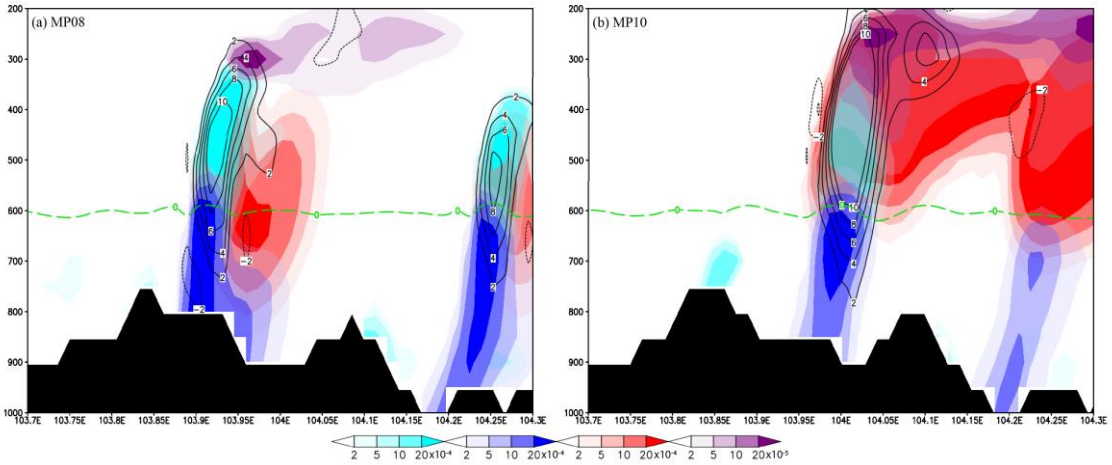

Figure 7. Vertical-longitude section across (a) 22.22°N by the Thompson scheme and (b) 22.25°N by the Morrison scheme at 23:00 local time on 17 March 2020. Shades are mixing ratios ($kg.kg^{-1}$) of cloud water (cyan), rain (blue), graupel (red), and ice (purple). Black dotted lines represent the vertical velocity ($m.s^{-1}$), and the black shade represents the topography. The green dashed lines denote 0°C isotherm

4. Conclusions

This study provides insight into the predictability of hail coverage (i.e., areas with hail diameter > 5 mm) and diameter by the WRF model with the Thompson and Morrison microphysical schemes (i.e., MP08 and MP10) for the hail event occurring in Lai Chau, Lao Cai, and Son La in the evening of 17 March 2020, which had the maximum reported diameter of about 3–4 cm. Comparisons of 18–30 hours lead-time forecasts with the radar observations indicate that WRF can predict hail coverage relatively well, but the timing of the predicted hails is Compared with the observations, 1–3 hours later (i.e., in Lai Chau and Lao Cai) or sooner (i.e., in Son La). However, this error in timing is quite acceptable in operational mode with day-ahead lead time (Gagne et al., 2015).

Among the four predicted indices and variables given by each microphysical scheme, the UH index generally appears to produce better hail forecasts regarding FSS (Gagne et al., 2017; Labriola et al., 2019a). However, the HAILCAST submodel using MP10 gives the best hail coverage and diameter forecasts compared to the radar observations and field reports. The variable D_{Th} of the Thompson algorithm appears to have almost no skill because of many false alarms. MP10 helps the two indices UH and CTG and the variable D_{Hc} to make forecasts significant on the horizontal scales > 25–45 km, which are reasonable compared with the skill-attaining scales of 20–50 km or larger of Labriola et al. (2017). In contrast, only the two indices, UH and CTG, are significant on the horizontal scales > 60–70 km in the case of MP08. Therefore, this study suggests that the former microphysical scheme is better than the latter, and a recommendation should be made here for further investigations of hail predictions in Vietnam.

Although the predicted indices and variables have skill in hail coverage prediction as mentioned above, there exist disadvantages, such as they are not developed to predict hail (i.e., UH and CTG) directly or strongly depend on microphysical parameterization schemes (CTG, D_{Th}, and D_{Hc}). Meanwhile, microphysical parameterizations still have limits in approximating the growth rates of hydrometeors, especially in thunderstorms. Therefore, improvements in MP are essential to improving hail predictability using NWP models. It is also necessary to install hailpad networks in Northwestern Vietnam and Central Highlands, where hail often occurs. This could help to verify hail predictability by NWP models (Malecic et al., 2022). On the other hand, field reports on hail size are still important information for evaluating hail forecasts (Allen et al., 2020).

In this case study, the predicted hailstorms could occur in the environments of moderate CAPE instead of strong CAPE as expected. However, VIMFC must be very strong to fuel the hailstorms, and a lifting mechanism by high mountains is vital to trigger them. This implies that forecasts based on the CAPE index alone may miss hailstorms. On the other hand, the eastward propagation of the hailstorms could be induced by robust VIMFC centers along their leading edge.

Vertical-longitude sections across the strongest predicted hailstorms indicate that MP08 predicts weaker updraft velocities than MP10, leading to the fact that the UH index given by MP08 predicts weaker hail. However, this scheme may induce more convective cells that may bring hail. Finally, MP10 appears to predict main convective cells better, creating necessary conditions for the HAILCAST submodel to provide hail forecasts that best agree with the radar observations and field reports on the surface hail size. This is because HAILCAST can use

kinematic and microphysical factors to predict maximum hail size at the surface.

Acknowledgments

This research is funded by the University of Science, Vietnam National University, Hanoi, under project number TN.22.13.

References

Adams-Selin, R.D.A.J. Clark, C.J. Melick, S.R. Dembek, I.L. Jirak, C.L. Ziegler, 2019. Evolution of WRF-HAILCAST during the 2014-16 NOAA/Hazardous Weather Testbed Spring Forecasting Experiments. Wea. Forecasting, 34, 61–79. https://doi.org/10.1175/WAF-D-18-0024.1

Adams-Selin R.D., C.L. Ziegler, 2016. Forecasting Hail Using a One-Dimensional Hail Growth Model within WRF. Mon. Wea. Rev., 144, 4919–4939. https://doi.org/10.1175/MWR-D-16-0027.1

Allen J.T., et al., 2020. Understanding hail in the Earth system. Reviews of Geophysics, 58, e2019RG000665. https://doi.org/10.1029/2019RG000665.

Banacos P.C., D.M. Schultz, 2005. The use of moisture flux convergence in forecasting convective initiation: Historical and operational perspectives. Wea. Forecasting, 20, 351–366.

Brimelow, J.C.G.W. Reuter, E.R. Poolman, 2002. Modeling Maximum Hail Size in Alberta Thunderstorms. Wea. Forecasting, 17, 1048–1062. https://doi.org/10.1175/1520-0434(2002)017<1048:MMHSIA>2.0.CO;2.

Duy D.M., Truong N.M. 2022. Numerical Reforecast of Severe Hailstorms in Eastern North Vietnam in 24–25/01/2020. J. Hydro-Meteorol., 737(5), 1–14 (in Vietnamese). Doi: 10.36335/VNJHM.2022(737).1-14.

Gagne D.J.A. McGovern, S.E. Haupt, R.A. Sobash, J.K. Williams, M. Xue, 2017. Storm-Based Probabilistic Hail Forecasting with Machine Learning Applied to Convection-Allowing Ensembles. Wea. Forecasting, 32, 1819–1840. https://doi.org/10.1175/WAF-D-17-0010.1.

Gagne D., A. McGovern, J. Brotzge, J. Correia, 2015. Day-Ahead Hail Prediction Integrating Machine Learning with Storm-Scale Numerical Weather Models. 29(2), 3954–3960, Twenty-Seventh Conference on Innovative Applications of Artificial Intelligence.

Helmus J.J., Collis S.M., 2016. The Python ARM Radar Toolkit (Py-ART), a Library for Working with Weather Radar Data in the Python Programming Language. Journal of Open Research Software, 4(1), e25. https://doi.org/10.5334/jors.119.

Hoat D., H. Quyen, L.N. Hong, V.D. Thanh, N.C., 2023. Building Rainfall Estimation Tool From Radar Reflectivity Using Artificial Intelligence Technique. J. Hydro-Meteorol., 747, 70–80 (in Vietnamese). Doi: 10.36335/VNJHM.2023(747).70-80.

Jewell R., J. Brimelow, 2009. Evaluation of Alberta Hail Growth Model Using Severe Hail Proximity Soundings from the United States. Wea. Forecasting, 24, 1592–1609, https://doi.org/10.1175/2009WAF2222230.1.

John S. Kain, Steven J. Weiss, David R. Bright, Michael E. Baldwin, Jason J. Levit, Gregory W. Carbin, Craig S. Schwartz, Morris L. Weisman, Kelvin K. Droegemeier, Daniel B. Weber, Kevin W. Thomas, 2008. Some Practical Considerations Regarding Horizontal Resolution in the First Generation of Operational Convection-Allowing NWP. Wea. Forecasting, 23, 931–952. https://doi.org/10.1175/WAF2007106.1.

Labriola J., N. Snook, M. Xue, K.W. Thomas, 2019a. Forecasting the 8 May 2017 Severe Hail Storm in Denver, Colorado, at a Convection-Allowing Resolution: Understanding Rimed Ice Treatments in Multimoment Microphysics Schemes and Their Effects on Hail Size Forecasts. Mon. Wea. Rev., 147, 3045–3068. https://doi.org/10.1175/MWR-D-18-0319.1.

Labriola J., N. Snook, Y. Jung, M. Xue, 2019b. Explicit Ensemble Prediction of Hail in 19 May 2013 Oklahoma City Thunderstorms and Analysis of Hail Growth Processes with Several Multimoment Microphysics Schemes. Mon. Wea. Rev., 147, 1193–1213. https://doi.org/10.1175/MWR-D-18-0266.1.

Labriola J., N. Snook, Y. Jung, M. Xue, 2020. Evaluating Ensemble Kalman Filter Analyses of Severe Hailstorms on 8 May 2017 in Colorado: Effects of State Variable Updating and

Multimoment Microphysics Schemes on State Variable Cross Covariances. Mon. Wea. Rev., 148, 2365–2389. https://doi.org/10.1175/MWR-D-19-0300.1.

Labriola J., N. Snook, Y. Jung, B. Putnam, M. Xue, 2017. Ensemble Hail Prediction for the Storms of 10 May 2010 in South-Central Oklahoma Using Single- and Double-Moment Microphysical Schemes. Mon. Wea. Rev., 145, 4911–4936. https://doi.org/10.1175/MWR-D-17-0039.1.

Li Z., P. Zuidema, P. Zhu, H. Morrison, 2015. The Sensitivity of Simulated Shallow Cumulus Convection and Cold Pools to Microphysics. J. Atmos. Sci., 72, 3340–3355. https://doi.org/10.1175/JAS-D-14-0099.1.

Luo L., M. Xue, K. Zhu, B. Zhou, 2017. Explicit prediction of hail using multimoment microphysics schemes for a hailstorm of 19 March 2014 in eastern China, J. Geophys. Res. Atmos., 122, 7560–7581. Doi: 10.1002/2017JD026747.

Luo L., M. Xue, K. Zhu, B. Zhou, 2018: Explicit Prediction of Hail in a Long-Lasting Multicellular Convective System in Eastern China Using Multimoment Microphysics Schemes. J. Atmos. Sci., 75, 3115–3137. https://doi.org/10.1175/JAS-D-17-0302.1.

Malecic B., M.T. Prtenjak, K. Horvath, D. Jelic, P.M. Jurkovic, K. Corko, N.S. Mahovic, 2022. Performance of HAILCAST and the Lightning Potential Index in simulating hailstorms in Croatia in a mesoscale model - Sensitivity to the PBL and microphysics parameterization schemes. Atmospheric Research, 272, 106143.

Melcón P. Merino, A. Sánchez, J.L. López L., García-Ortega E., 2017. Spatial Patterns of Thermodynamic Conditions of Hailstorms in Southwestern France. Atmospheric Research, 189(1), 111–126. https://doi.org/10.1016/j.atmosres.2017.01.011.

Minh N.H., Dung P.T., Van V.T., T. Hai, D.V. Khiem, MV, 2023. Accuracy Improvement of Flood Forecast by Blending Radar-based Rainfall Prediction with Numerical Weather Prediction Rainfall Product. J. Hydro-Meteorol, 751(7), 91–101 (in Vietnamese). Doi: 10.36335/VNJHM.2023(751), 91–101.

Mittermaier M.P., 2021. A "Meta" Analysis of the Fractions Skill Score: The Limiting Case and Implications for Aggregation. Mon. Wea. Rev., 149, 3491–3504. https://doi.org/10.1175/MWR-D-18-0106.1.

Morrison H., J.A. Curry, V.I. Khvorostyanov, 2005. A New Double-Moment Microphysics Parameterization for Application in Cloud and Climate Models. Part I: Description. J. Atmos. Sci. 62, 1665–1677, https://doi.org/10.1175/JAS3446.1.

NOAA Global Forecast System (GFS). https://registry.opendata.aws/noaa-gfs-bdp-pds accessed on 15 August, 2023.

Kiel L. Ortega, John M. Krause, Alexander V. Ryzhkov, 2016. Polarimetric Radar Characteristics of Melting Hail. Part III: Validation of the Algorithm for Hail Size Discrimination. J. Appl. Meteor. Climatol., 55, 829–848. https://doi.org/10.1175/JAMC-D-15-0203.1.

Hyang Suk Park, A.V. Ryzhkov, D.S. Zrnić, Kyung-Eak Kim, 2009. The Hydrometeor Classification Algorithm for the Polarimetric WSR-88D: Description and Application to an MCS. Wea. Forecasting, 24, 730–748. https://doi.org/10.1175/2008WAF2222205.1.

Powers J.G., et al., 2017. The Weather Research and Forecasting Model: Overview, System Efforts, and Future Directions. Bull. Amer. Meteor. Soc., 98, 1717–1737, https://doi.org/10.1175/BAMS-D-15-00308.1.

Quyet L.D., Nghi V.V., Giam N.M., 2011. Detecting Thunderstorms using Doppler Weather Radar. J. Hydro-Meteorol, 31–37 (in Vietnamese). https://vjol.info.vn/index.php/TCKHTV/article/view/60493/50765 accessed on 15 August, 2023.

Roberts N.M., Lean H.W., 2008. Scale-Selective Verification of Rainfall Accumulations from High-Resolution Forecasts of Convective Events. Monthly Weather Review, 136(1), 78–97. https://doi.org/10.1175/2007MWR2123.1.

Alexander V. Ryzhkov, Matthew R. Kumjian, Scott M. Ganson, Pengfei Zhang, 2013. Polarimetric Radar Characteristics of Melting Hail. Part II: Practical Implications. J. Appl. Meteor. Climatol., 52, 2871–2886. https://doi.org/10.1175/JAMC-D-13-074.1.

Skamarock W.C., et al., 2021. A Description of the Advanced Research WRF Model Version 4.3 (No. NCAR/TN-556+STR). Doi: 10.5065/1dfh-6p97.

Snook N., Jung Y., Brotzge J., Putnam B., Xue M., 2016. Prediction and Ensemble Forecast Verification of Hail in the Supercell Storms of 20 May 2013. Wea. Forecasting, 31(3), 811–825. https://doi.org/10.1175/WAF-D-15-0152.1.

Sobash R.A., Romine G.S., Schwartz C.S., 2020. A Comparison of Neural-Network and Surrogate-Severe Probabilistic Convective Hazard Guidance Derived from a Convection-Allowing Model. Wea. Forecasting, 35(5), 1981–2000. https://doi.org/10.1175/WAF-D-20-0036.1.

Stull R., 2017. Practical Meteorology: An Algebra-based Survey of Atmospheric Science -version 1.02b. Univ. of British Columbia, 940p. ISBN 978-0-88865-283-6.

Thang N.V., Kien T.B., Thuc T.D., Thang V.V., 2020. An Investigation into the Causes of the Hailstorm over the Nothern Viet Nam from 24th to 25th January 2020. Journal of Climate Change Science, 13, 1–10 (in Vietnamese). https://vjol.info.vn/index.php/TCKHBDKH/article/view/57843/48258 accessed on 15 August, 2023.

Thanh C., Nhu Quy N., Van Khiem M., 2018. Assessing the Rain Estimate from the Feflectivity of Nha Be Radar. VNU Journal Of Science: Earth And Environmental Sciences, 34(1S), 10–17 (in Vietnamese). Doi: 10.25073/2588-1094/vnuees.4330.

Thompson G., Field P.R., Rasmussen R.M., Hall W.D. 2008. Explicit Forecasts of Winter Precipitation Using an Improved Bulk Microphysics Scheme. Part II: Implementation of a New Snow Parameterization. Mon. Wea. Rev., 136(12), 5095–5115. https://doi.org/10.1175/2008MWR2387.1.

Ulbrich C.W., 1983. Natural Variations in the Analytical Form of the Raindrop Size Distribution. J. Appl. Meteor. Climatol, 22(10), 1764–1775. https://doi.org/10.1175/1520-0450(1983)022<1764:NVITAF>2.0.CO;2.

Van Weverberg K., et al., 2013. The Role of Cloud Microphysics Parameterization in the Simulation of Mesoscale Convective System Clouds and Precipitation in the Tropical Western Pacific. J. Atmos. Sci., 70, 1104–1128. https://doi.org/10.1175/JAS-D-12-0104.1.

Vietnam Meteorological and Hydrological Administration. http://vmha.gov.vn/public/index.php/tin-tuc-khcn-120/dien-bien-mua-dong-lo%3Fc-mua-da-ngay-17-18-va-21-den-23-thang-3-nam-2020-tren-khu-vuc-cac-tinh-bac-bo-va-bac-trung-bo-8469.html accessed on 15 August, 2023.

Wu W., W. Huang, L. Deng, C. Wu, 2022. Investigation of Maximum Hail-Size Forecasting Using Bulk Microphysics Schemes. Mon. Wea. Rev., 150, 2503–2525, https://doi.org/10.1175/MWR-D-21-0312.1.

Zomeren J.V., A.V. Delden, 2007. Vertically integrated moisture flux convergence as a predictor of thunderstorms, Atmospheric Research, 83(2), 435–445.